

Fundamentals of Vibration Analysis and Vibroacoustics
Module 2 - Vibroacoustics of Musical Instruments
Assignment 1 - Axial vibration of undamped and
damped bars

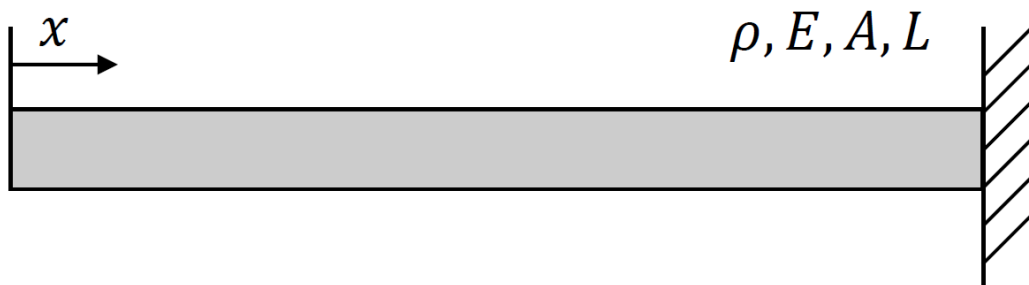
Bombaci Nicola 10677942

Fantin Jacopo 10591775

Intagliata Emanuele 10544878

June 2020

System schematic and parameters



$$\rho = 2700 \text{ kg/m}^3, E = 70 \text{ GPa}, L = 2 \text{ m}, b = h = 0.05 \text{ m}$$

1) Natural frequencies and mode shapes in free-fixed configuration

Starting from the one-dimensional wave equation and applying it for the axial displacement $s(x, t)$ of point at position x at time t :

$$\frac{\partial^2 s(x, t)}{\partial x^2} = \frac{1}{c^2} \frac{\partial^2 s(x, t)}{\partial t^2}$$

We already know that a solution to the equation is the standing wave expression, where space and time dependencies are separated by the mode shape function $\Phi(x)$ and the complex exponential $G(t)$:

$$s(x, t) = \Phi(x) G(t) = (A \sin(kx) + B \cos(kx)) e^{j\omega t}$$

The bar is in free-fixed condition, so we've got a natural boundary condition at the left end that imposes the axial force N be null because the end is free and there is no constraint being able to react to the horizontal force, and a geometric boundary condition at the right end, being this fixed:

$$\begin{cases} N(0, t) = E S \frac{\partial s(x, t)}{\partial x} \Big|_{x=0} = 0 \Rightarrow E S A k e^{j\omega t} = 0 \Rightarrow A = 0 \text{ (} k = 0 \text{ is a trivial solution)} \\ s(L, t) = 0 \Rightarrow B \cos(kL) = 0 \Rightarrow k^{\text{fr-fx}(i)} = \frac{2i-1}{2L}\pi, i = 1, 2, \dots, \infty \end{cases}$$

where S denotes the area of the bar's cross-section and N the normal axial load. From the second condition, the natural frequencies can be directly retrieved:

$$f_n^{\text{fr-fx}(i)} = \frac{\omega_n^{\text{fr-fx}(i)}}{2\pi} = \frac{c k^{\text{fr-fx}(i)}}{2\pi} = \frac{2i-1}{4L} \sqrt{\frac{E}{\rho}}, i = 1, 2, \dots, \infty$$

Our analysis is restricted to the frequency band $[0, f_{\max}] = [0, 10k]$ Hz, so i assumes values within a finite set of indices:

$$\begin{aligned} f_{\max} &= \frac{2i_{\max}^{\text{fr-fx}} - 1}{4L} \sqrt{\frac{E}{\rho}} \\ \Rightarrow \lfloor i_{\max}^{\text{fr-fx}} \rfloor &= \left\lfloor 2L f_{\max} \sqrt{\frac{\rho}{E}} + \frac{1}{2} \right\rfloor = \lfloor 8.35 \rfloor = 8 \end{aligned}$$

So $i = 1, 2, \dots, 8$ and the resulting natural frequencies are

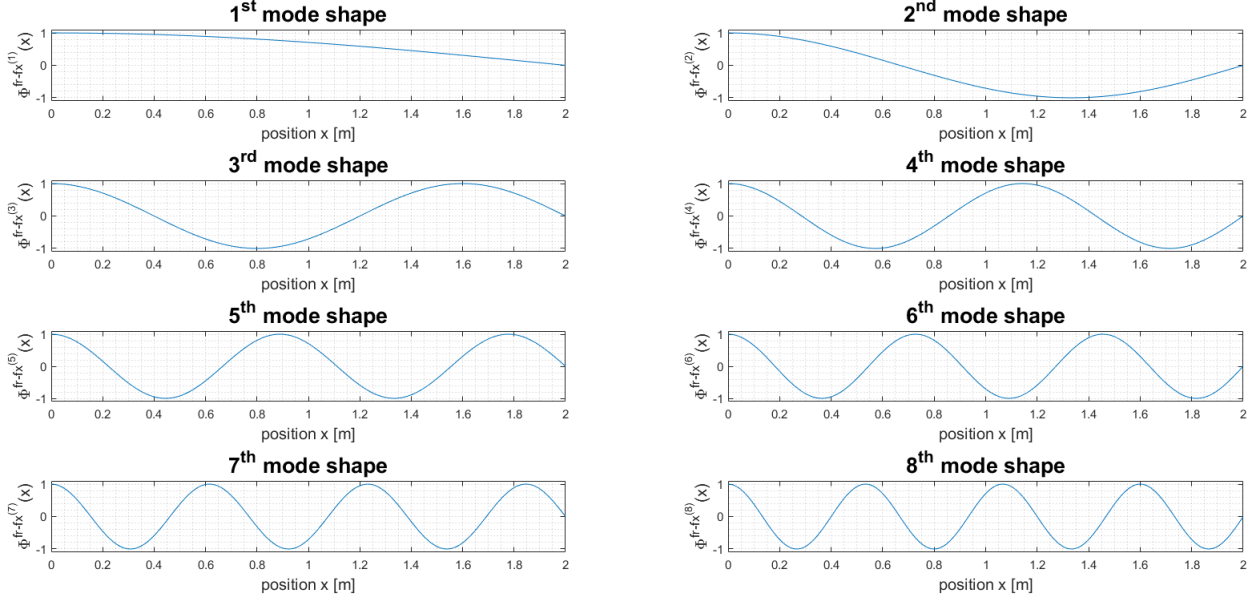
$$\mathbf{f}_n^{\text{fr-fx}} = [636.47 \ 1909.40 \ 3182.30 \ 4455.30 \ 5728.20 \ 7001.20 \ 8274.10 \ 9547.00]$$

The mode shapes $\Phi^{\text{fr-fx}(i)}(x)$ are then, considering the constant coefficient $B = 1$,

$$\Phi^{\text{fr-fx}(i)}(x) = \cos(k^{\text{fr-fx}(i)} x) = \cos\left(\frac{2i-1}{2L}\pi x\right), i = 1, 2, \dots, 8$$

We hereby show them plotting the longitudinal oscillation amplitude of each point of the bar versus the points position. As expected, the oscillation of the free end always has maximum amplitude.

Mode shapes
Free-fixed configuration



2) Natural frequencies and mode shapes in free-free configuration

Differently, in a free-free configuration of the bar the boundary condition on the normal force N is applied to the right end of the bar too:

$$\begin{cases} N(0, t) = E S \frac{\partial s(x, t)}{\partial x} \Big|_{x=0} = 0 \Rightarrow E S A k e^{j\omega t} = 0 \Rightarrow A = 0 \text{ (} k = 0 \text{ is a trivial solution)} \\ N(L, t) = E S \frac{\partial s(x, t)}{\partial x} \Big|_{x=L} = 0 \Rightarrow -E S B k \sin(kL) = 0 \Rightarrow \sin(kL) = 0 \\ \Rightarrow k^{\text{fr-fr}(i)} = \frac{i}{L}\pi, i = 0, 1, \dots, \infty \end{cases}$$

So the natural frequencies are computed from $k^{\text{fr-fr}(i)}$ as before:

$$f_n^{\text{fr-fr}(i)} = \frac{\omega_n^{\text{fr-fr}(i)}}{2\pi} = \frac{c k^{\text{fr-fr}(i)}}{2\pi} = \frac{i}{2L} \sqrt{\frac{E}{\rho}}, i = 0, 1, \dots, \infty$$

This time the maximum value for index i is

$$\begin{aligned} f_{\max} &= \frac{i_{\max}^{\text{fr-fr}}}{2L} \sqrt{\frac{E}{\rho}} \\ \Rightarrow \lfloor i_{\max}^{\text{fr-fr}} \rfloor &= \left\lfloor 2L f_{\max} \sqrt{\frac{\rho}{E}} \right\rfloor = \lfloor 7.86 \rfloor = 7 \end{aligned}$$

So $i = 0, 1, \dots, 7$ and the corresponding natural frequencies are

$$\mathbf{f}_n^{\text{fr-fr}} = [0 \ 1272.9 \ 2545.9 \ 3818.8 \ 5091.8 \ 6364.7 \ 7637.6 \ 8910.6]$$

The number of resonances within f_{\max} is the same, but the most important consideration is about the fact the system has now a resonance at $f = 0$, which means a fixed amount of longitudinal displacement is added to the displacement of each point of the bar during the vibration. This value, constant in time, is called rigid motion. Intuitively, it makes perfect sense as the bar is in free-free configuration, and applying a constant force at one of the two ends, the whole bar will rigidly move in the direction of the force. The fixed-fixed configuration shows a zero-frequency component too, but it doesn't correspond to a rigid motion different from zero, but rather to absence of motion, therefore it's not includable among the system's resonances but it's rather a trivial solution of the equation of motion. The second consideration is that, while in the free-fixed case the resonance frequencies are odd integer multiples of the fundamental, in the free-free case these are all the integer multiples of the fundamental, both even and odd, which is twice that of the first case. In other words, naming $f_0 = 636.47 \text{ Hz}$ the fundamental frequency of the free-fixed configuration, in the first case the resonances are

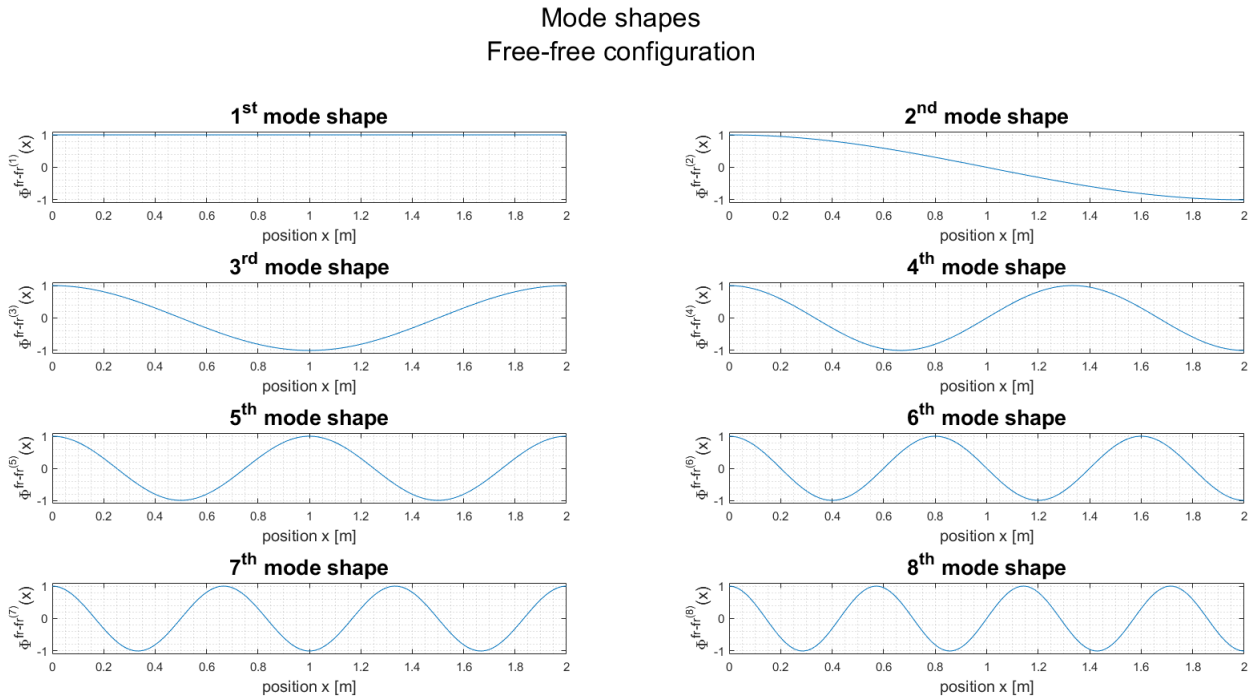
$$\mathbf{f}_n^{\text{fr-fr}} = [f_0 \ 3f_0 \ 5f_0 \ 7f_0 \ 9f_0 \ 11f_0 \ 13f_0 \ 15f_0]$$

while in the second case

$$\mathbf{f}_n^{\text{fr-fr}} = [0 \ 2f_0 \ 4f_0 \ 6f_0 \ 8f_0 \ 10f_0 \ 12f_0 \ 14f_0]$$

Just like before, the resulting mode shapes $\Phi^{\text{fr-fr}^{(i)}}(x)$ are computed and plotted considering $B = 1$.

$$\Phi^{\text{fr-fr}^{(i)}}(x) = \cos(k^{\text{fr-fr}^{(i)}} x) = \cos\left(\frac{i}{L}\pi x\right), i = 0, 1, \dots, 7$$



3) Frequency Response Functions in free-fixed configuration

For computing the system's FRFs, we're considering a harmonic force $F(t) = F_0 e^{j\omega t}$ acting at the bar free end, so the application point is at $\bar{x} = 0$, while the bar points for which the FRF is computed are at $\bar{x} = \frac{L}{2}$ and $\bar{x} = \frac{L}{5}$. We're asked to find the FRFs in three different cases.

Case 1: undamped bar (standing wave solution)

Considering the bar as not affected by energy losses during its vibration, a solution of the wave equation is sought, resulting in non-attenuating standing waves superposition. Like we did for the natural frequencies of the bar, we find the coefficients A and B appearing in the expression for $\Phi(x)$ imposing the same boundary conditions as in the free-fixed condition, but accounting for the external harmonic excitation too:

$$\begin{cases} N(0, t) = E S \frac{\partial s(x, t)}{\partial x} \Big|_{x=0} + F_0 e^{j\omega t} = 0 \Rightarrow E S A k e^{j\omega t} + F_0 e^{j\omega t} = 0 \Rightarrow A = -\frac{F_0}{E S k} \\ s(L, t) = 0 \Rightarrow -\frac{F_0}{E S k} \sin(kL) + B \cos(kL) = 0 \Rightarrow B = \frac{F_0 \sin(kL)}{E S k \cos(kL)} \end{cases}$$

$$\Rightarrow s(x, t) = (A \sin(kx) + B \cos(kx)) e^{j\omega t} = \frac{\sin(k(L-x))}{E S k \cos(kL)} F_0 e^{j\omega t} \Rightarrow \frac{\sin(k(L-x))}{E S k \cos(kL)} F(t)$$

from which the FRF can be retrieved, considering the frequency dependency in place of the time dependency:

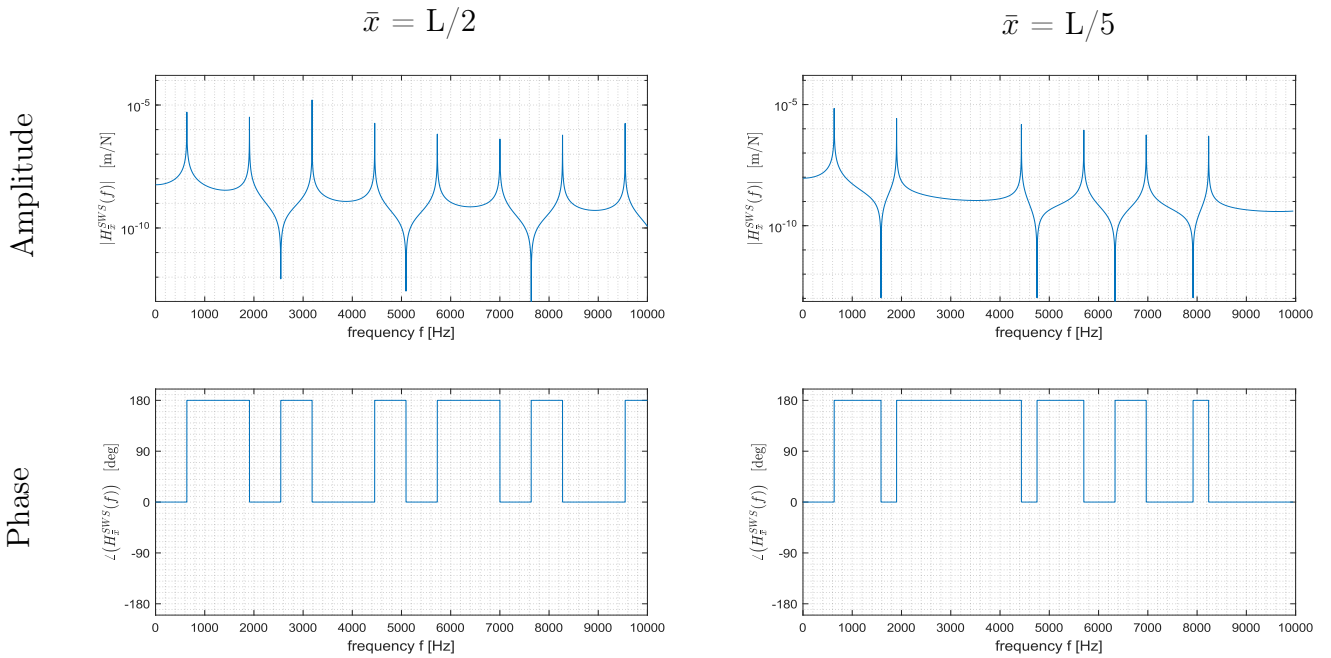
$$H^{SWS}(\omega) = \frac{s(x, \omega)}{F(\omega)} = \frac{\sin(k(L-x))}{E S k \cos(kL)}$$

The FRF connecting the specific point \bar{x} on the x-axis to the force applied at the free end is then:

$$H_{\bar{x}}^{SWS}(\omega) = H^{SWS}(\omega) \Big|_{x=\bar{x}} = \frac{\sin(k(L-\bar{x}))}{E S k \cos(kL)} \quad (1)$$

We hereby show the amplitude and phase plots for both the points we want to compute the response of. Note that, for $\bar{x} = \frac{L}{5}$, two resonances are missing, precisely those of mode 3 and 8, indicating that these modes are non-observable modes in point $\bar{x} = \frac{L}{5}$. In this case, the poles of the FRF corresponding to the resonances of modes 3 and 8 are compensated by the zeros given by the anti-resonances of this nodal point. This comes in accordance with the mode shapes we found in section [1]. The point $\bar{x} = \frac{L}{5} = 0.4 \text{ m}$ is indeed a node for mode shapes 3 and 8, while $\bar{x} = \frac{L}{2}$ is a node for no mode, due to the asymmetric boundary conditions we imposed, due to asymmetric bar configuration in turn. The peak values numerically represent an infinite value, obtained at resonance in an undamped condition. The anti-resonances change too from one measurement point to the other, but this is true in general since the zeros of the transfer function necessarily vary according to \bar{x} , in contrast to poles (so, resonances) which, apart from the case of non-observable modes for certain nodal positions, are always the same for all the output positions as the denominator of the transfer function doesn't depend on it.

FREQUENCY RESPONSE FUNCTIONS
CASE 1: UNDAMPED BAR (STANDING WAVE SOLUTION)



Case 2: damped bar (wave propagation solution)

In this second case, the bar is damped, so the energy loss factor η is introduced. This represents the viscoelasticity of the bar, which is now not purely elastic as in an undamped one, and is comprised in a new, complex, Young's modulus, which leads to a new wave equation:

$$\begin{aligned} E' &= E(1 + j\eta) \Rightarrow E' \frac{\partial^2 s(x, t)}{\partial x^2} = \rho \frac{\partial^2 s(x, t)}{\partial t^2} \\ \Rightarrow c' &= \sqrt{\frac{E'}{\rho}} = \sqrt{\frac{E(1 + j\eta)}{\rho}} = c \sqrt{1 + j\eta} \approx c \sqrt{\frac{1 + \frac{\eta^2}{4}}{1 + \frac{\eta^4}{16} + \frac{\eta^2}{2}}} + j \frac{\eta}{1 + \frac{\eta^4}{16} + \frac{\eta^2}{2}} = \frac{c}{1 - j\frac{\eta}{2}} \end{aligned}$$

where the approximation is valid for low loss factors, e.g. order of magnitude of 10^{-2} , which is our case. So the wavenumber is now

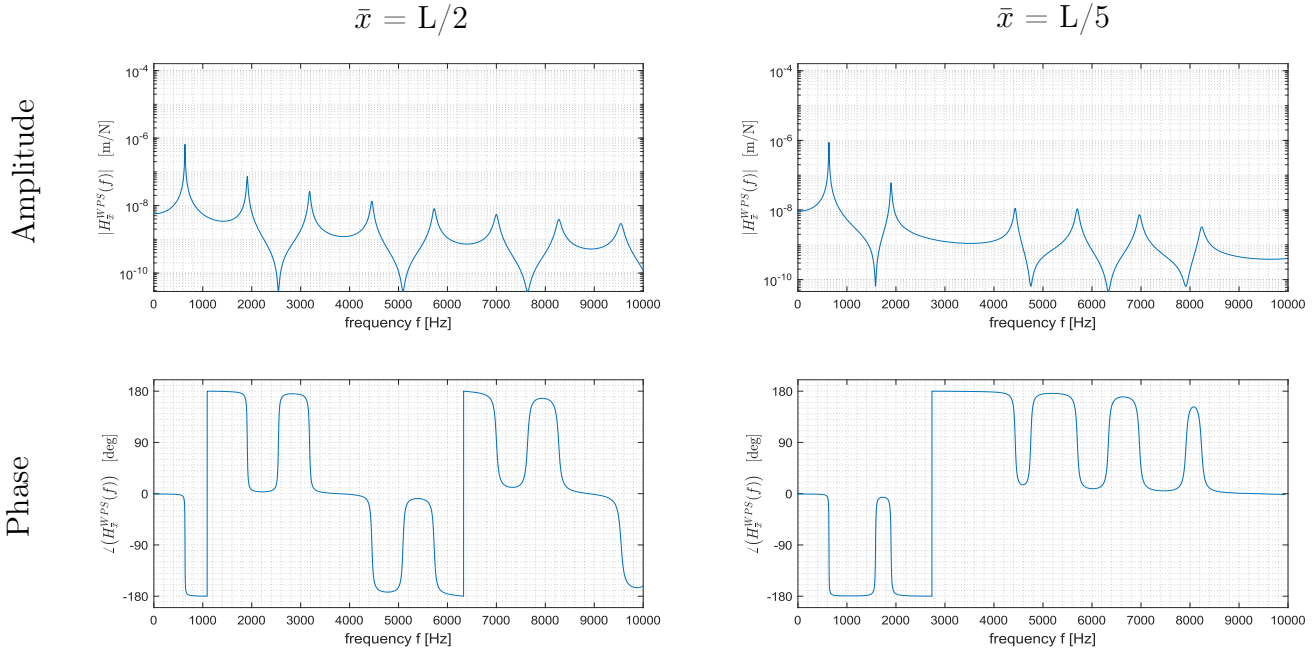
$$k' = \frac{\omega}{c'} = \frac{\omega}{c} \left(1 - j\frac{\eta}{2}\right) = k \left(1 - j\frac{\eta}{2}\right)$$

Applying the new value for Young's modulus and the wavenumber to the same FRF of the previous case (1), thus using the same boundary conditions as before, the new frequency response function is retrieved:

$$H_{\bar{x}}^{WPS}(\omega) = H^{WPS}(\omega)|_{x=\bar{x}} = \frac{\sin(k'(L - \bar{x}))}{E' S k' \cos(k'L)}$$

The corresponding magnitude and phase plots are depicted in the following figure. As we can see, the resonances are at the same frequencies as before, but the amplitude plot shows attenuated values due to the introduction of η , and the phase plot shows not perfectly vertical jumps now.

FREQUENCY RESPONSE FUNCTIONS
CASE 2: DAMPED BAR (WAVE PROPAGATION SOLUTION)



Case 3: damped bar (modal superposition approach)

Following a modal approach, we started from the theoretical result that allows us to find the bar point x_{out} 's steady-state oscillation amplitude as response to input external force $F(\omega)$ applied in point x_{in}

$$\begin{aligned} s(x_{\text{out}}, \omega) &= \sum_{i=1}^N \Phi^{(i)}(x) \Big|_{x_{\text{out}}} q_{0i} \\ &= \sum_{i=1}^N \frac{\Phi^{(i)}(x) \Big|_{x_{\text{out}}} \Phi^{(i)}(x) \Big|_{x_{\text{in}}} F_0}{-\omega^2 m^{(i)} + (1 + j\eta) k^{(i)}} \end{aligned}$$

In our case:

$$s(\bar{x}, \omega) = \sum_{i=1}^N \frac{\Phi^{\text{fr-fx}^{(i)}}(x) \Big|_{\bar{x}} \Phi^{\text{fr-fx}^{(i)}}(x) \Big|_0 F_0}{-\omega^2 m^{(i)} + (1 + j\eta) k^{(i)}}$$

Dividing both sides by F_0 the expression for the FRF is derived:

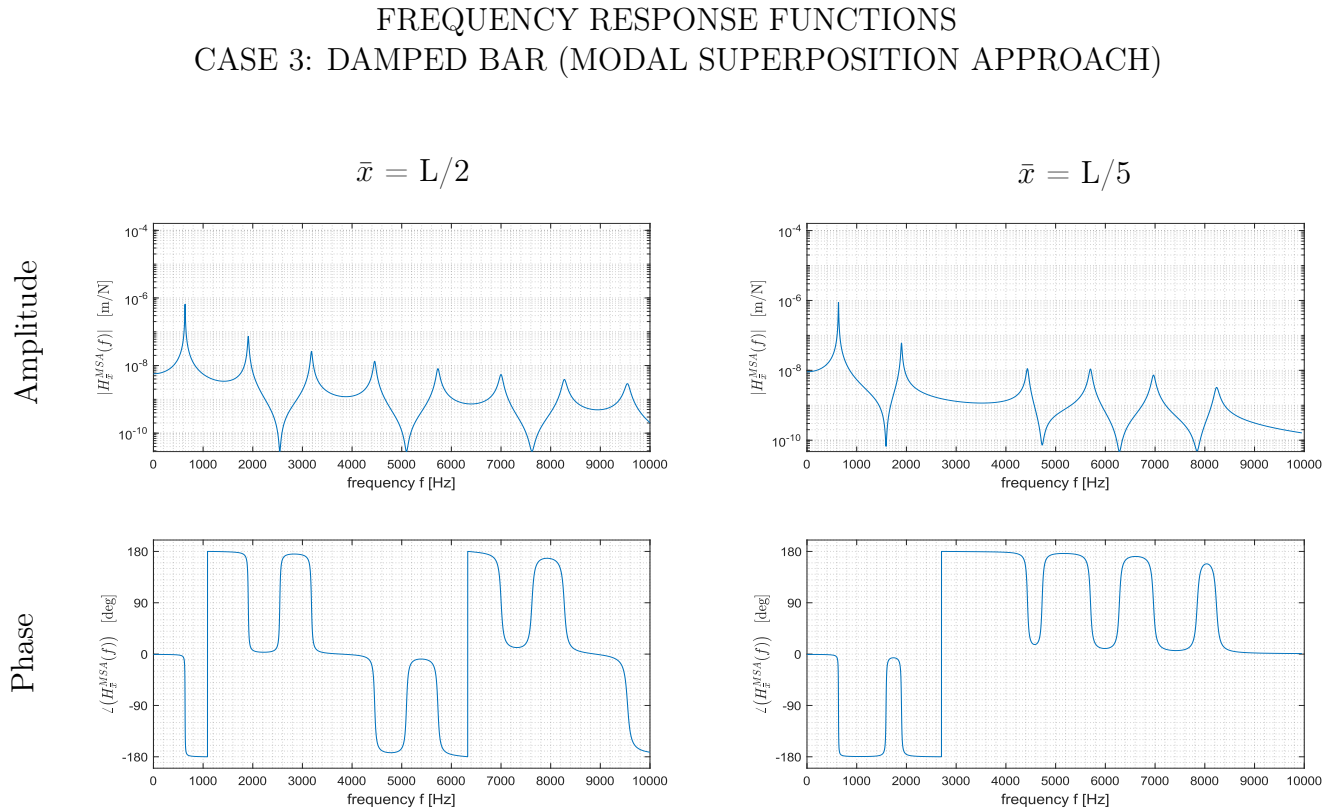
$$\begin{aligned} H_{\bar{x}}^{\text{MSA}} &= \sum_{i=1}^N \frac{\Phi^{\text{fr-fx}^{(i)}}(x) \Big|_{\bar{x}} \Phi^{\text{fr-fx}^{(i)}}(x) \Big|_0}{-\omega^2 m^{(i)} + (1 + j\eta) k^{(i)}} = \sum_{i=1}^N \frac{\cos(k^{\text{fr-fx}^{(i)}} x) \Big|_{\bar{x}} \cos(k^{\text{fr-fx}^{(i)}} x) \Big|_0}{-\omega^2 m^{(i)} + (1 + j\eta) k^{(i)}} = \\ &= \sum_{i=1}^N \frac{\cos(k^{\text{fr-fx}^{(i)}} \bar{x})}{-\omega^2 m^{(i)} + (1 + j\eta) k^{(i)}} \end{aligned}$$

The modal mass and stiffness $m^{(i)}$ and $k^{(i)}$ are the i-th element in the diagonal of the modal mass matrix and modal stiffness matrix respectively, and they have been retrieved as

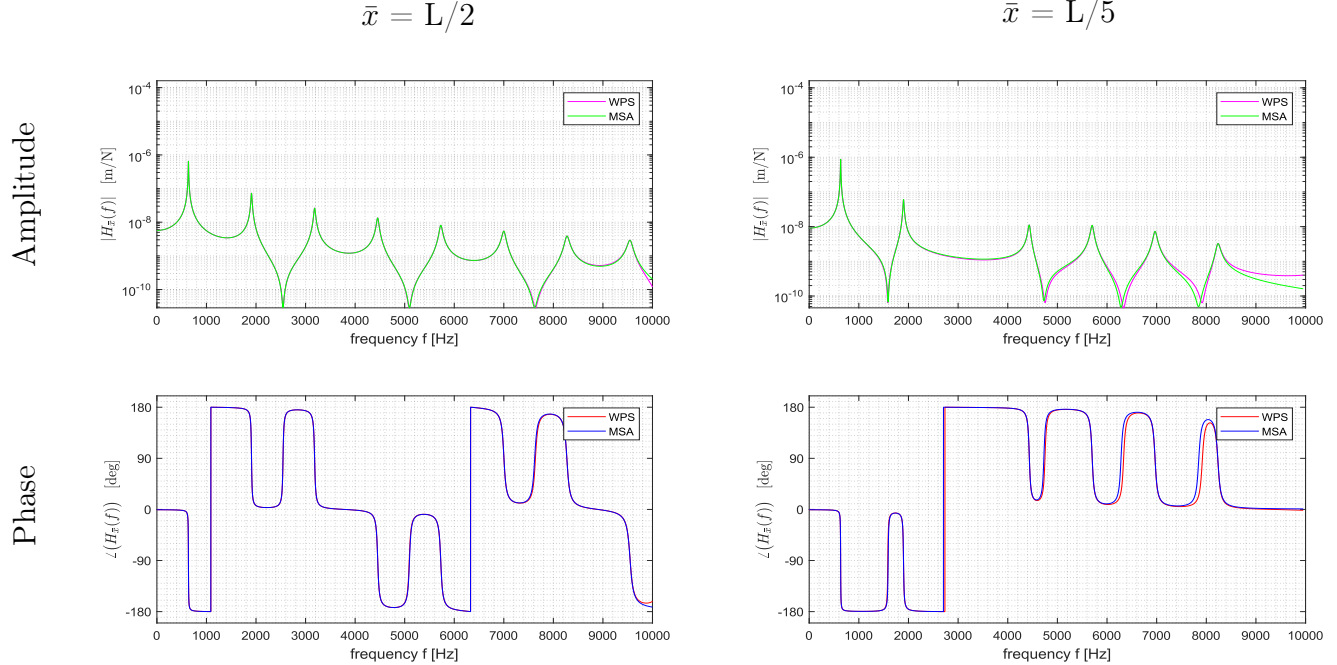
$$m^{(i)} = \int_0^L \mu \cos^2(k^{\text{fr-fx}}{}^{(i)} x) dx = \mu \frac{L}{2} + \frac{\sin(2Lk^{\text{fr-fx}}{}^{(i)})}{4 k^{\text{fr-fx}}{}^{(i)}}$$

$$k^{(i)} = \int_0^L E S \left(k^{\text{fr-fx}}{}^{(i)} \right)^2 \sin^2(k^{\text{fr-fx}}{}^{(i)} x) dx = E S \frac{L}{2} \left(k^{\text{fr-fx}}{}^{(i)} \right)^2 - \frac{\sin(2Lk^{\text{fr-fx}}{}^{(i)})}{4 k^{\text{fr-fx}}{}^{(i)}}$$

In the following plots we're showing the resulting FRFs and a comparison between those obtained through wave propagation solution and through modal superposition approach. The FRFs obtained using the two methods coincide very thoroughly in case of $\bar{x} = \frac{L}{2}$, beginning to diverge only at the very right end due to quasi-static contributions of modes higher than the 8th not taken into account for the modal approach, and generally thoroughly for $\bar{x} = \frac{L}{5}$, for which the difference between the two approaches shows up earlier than for $\bar{x} = \frac{L}{2}$. The reason for this must be the absence of two resonance peaks, that penalizes the modal approach more than in the other case.



FREQUENCY RESPONSE FUNCTIONS FREE-FIXED DAMPED BAR (WPS vs MSA)



4) Driving-point impedance in free-fixed configuration

Finally, the impedance computed at the force application point, i.e. $\bar{x} = 0$, is requested. The driving-point impedance in \bar{x} is defined as:

$$Z(\omega) = \frac{F(t)}{v(\bar{x}, t)} = \frac{F_0 e^{j\omega t}}{\frac{\partial s}{\partial t}(x, t)|_{\bar{x}}} = \frac{F_0}{v_0} \quad \text{with } \bar{x} = 0.$$

Two case studies are considered. In both cases we will consider a loss factor of $\eta = 0.01$.

Case 1: damped bar (wave propagation solution)

From the considerations we made in section 3) (case 2), we can write the axial displacement for a damped bar as:

$$s(x, t) = \frac{\sin(k'(L - x))}{E' S k' \cos(k'L)} F_0 e^{j\omega t}$$

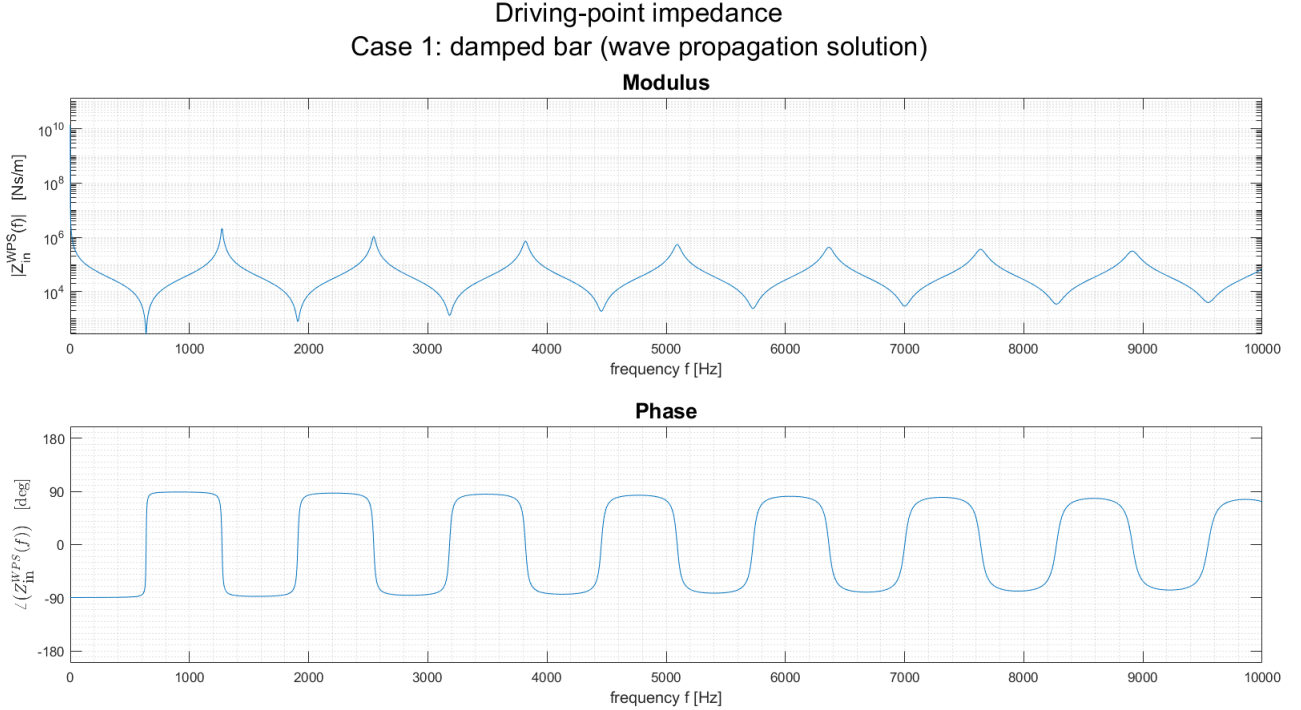
In this case we start from the wave propagation solution. The axial velocity at \bar{x} is:

$$v(\bar{x}, t) = \frac{\partial s}{\partial t}(x, t)|_{\bar{x}} = j\omega \frac{\sin(k'(L - \bar{x}))}{E' S k' \cos(k'L)} F_0 e^{j\omega t} = j\omega s(\bar{x}, t)$$

We can easily find that the driving-point impedance in $\bar{x} = 0$ is:

$$\begin{aligned} Z^{\text{WPS}}(\omega) &= \frac{E_0 e^{j\omega t}}{j\omega \frac{\sin(k'L)}{E' S k' \cos(k'L)} E_0 e^{j\omega t}} = -j \frac{k' E' S \cos(k'L)}{\omega \sin(k'L)} = \\ &= -j \frac{\sqrt{\frac{p}{E}} (1 - j\frac{\eta}{2}) E' S \cos(\sqrt{\frac{p}{E}} (1 - j\frac{\eta}{2}) L \omega)}{\sin(\sqrt{\frac{p}{E}} (1 - j\frac{\eta}{2}) L \omega)} \end{aligned}$$

This last expression is the one used in our MATLAB code to plot the driving-point impedance in the case of a damped bar, calculated starting from the wave propagation solution.



We can briefly comment the previous plot. Being the system damped, the driving-point impedance is complex. Therefore it does not go to zero at resonance and it does not go to infinite at anti resonance. Remembering that $Z(\omega) = Z_R + jZ_I = |Z| e^{j\phi}$, the average power input introduced into or removed from the system is different from zero. It is:

$$\overline{W} = \frac{1}{2} Z_R |v|^2$$

\overline{W} is maximum in correspondence to the resonances, where Z_R is maximum (as we can deduct from the phase plot).

Case 2: damped bar (modal superposition approach)

From the considerations we made in section 3 (case 3), we can write the axial displacement for a damped bar as:

$$s(\bar{x}, t) = F_0 e^{j\omega t} \sum_{i=1}^N \frac{\Phi^{\text{fr-fx}(i)}(x)|_{\bar{x}} \Phi^{\text{fr-fx}(i)}(x)|_0}{-\omega^2 m^{(i)} + (1 + j\eta) k^{(i)}}$$

In this case we start from the modal superposition approach. The axial velocity in \bar{x} is:

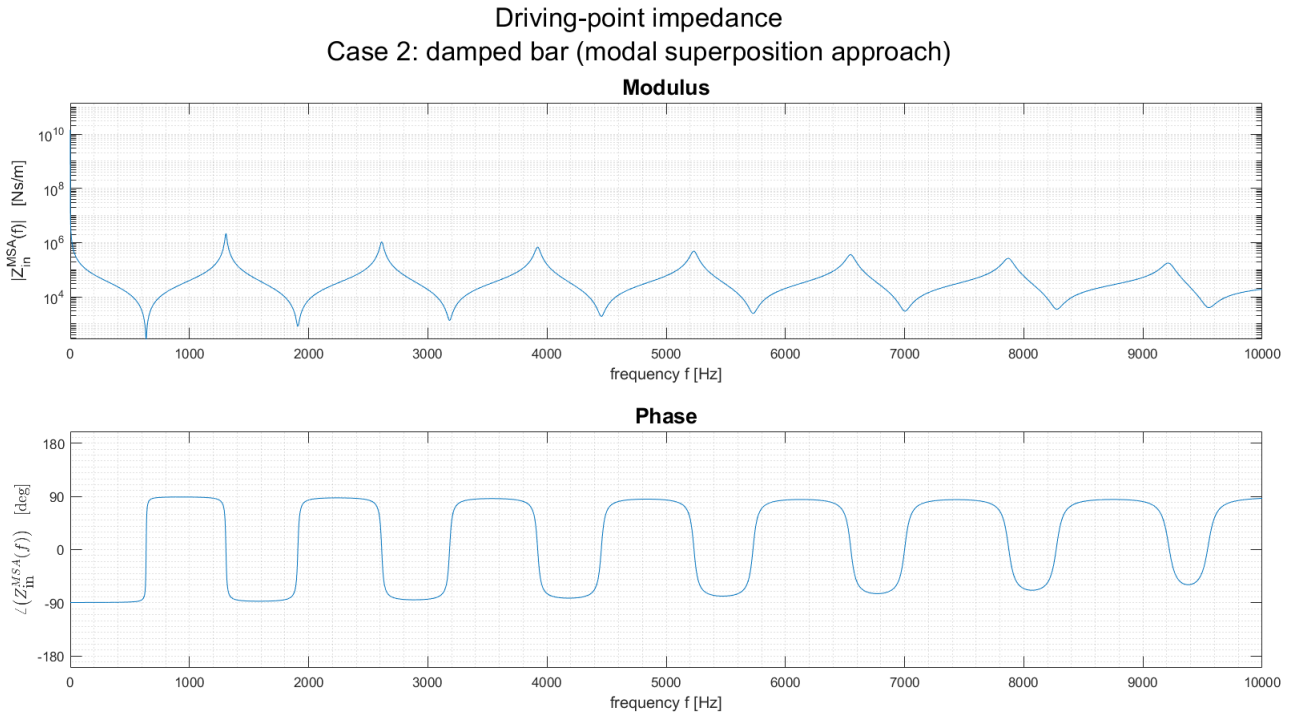
$$v(\bar{x}, t) = \frac{\partial s}{\partial t}(x, t)|_{\bar{x}} = j\omega F_0 e^{j\omega t} \sum_{i=1}^N \frac{\Phi^{\text{fr-fx}^{(i)}}(x)|_{\bar{x}} \Phi^{\text{fr-fx}^{(i)}}(x)|_0}{-\omega^2 m^{(i)} + (1 + j\eta) k^{(i)}} = j\omega s(\bar{x}, t)$$

The driving-point impedance is computed at the excitation point. Therefore $\Phi^{\text{fr-fx}^{(i)}}(x)|_{\bar{x}=0} = \Phi^{\text{fr-fx}^{(i)}}(x)|_0 = 1$. We can easily find that the driving-point impedance at $\bar{x} = 0$ is:

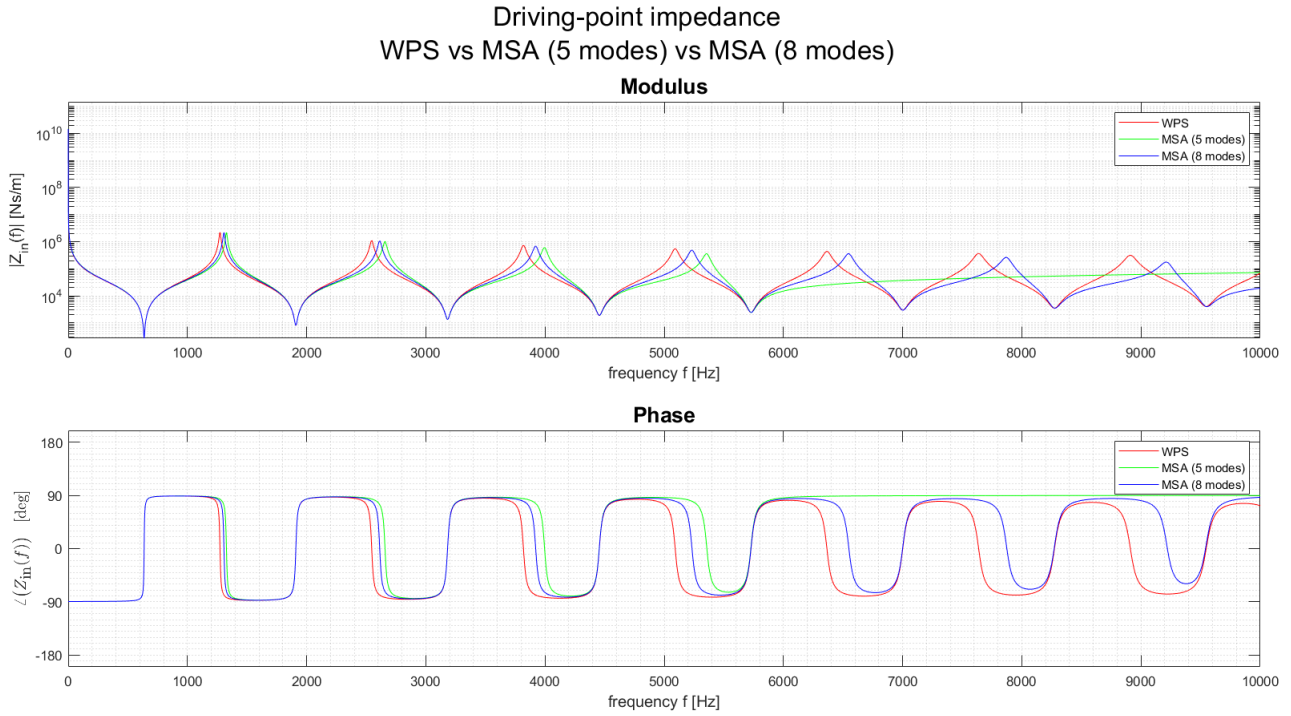
$$\begin{aligned} Z^{\text{MSA}}(\omega) &= \frac{E_0 e^{j\omega t}}{j\omega E_0 e^{j\omega t} \sum_{i=1}^N \frac{\Phi^{\text{fr-fx}^{(i)}}(x)|_{\bar{x}} \Phi^{\text{fr-fx}^{(i)}}(x)|_0}{-\omega^2 m^{(i)} + (1 + j\eta) k^{(i)}}} = \\ &= -j \frac{1}{\omega \sum_{i=1}^N \frac{1}{-\omega^2 m^{(i)} + (1 + j\eta) k^{(i)}}} \end{aligned}$$

The modal parameters $m^{(i)}$, $k^{(i)}$ are the ones calculated in section 3) (case 3).

This last expression is the one used in our MATLAB code to plot the driving-point impedance in the case of a damped bar, calculated starting from the modal superposition approach. In this case $N = 8$ modes are used.



Regarding this plot, we can derive the same conclusions as for case 1. It's interesting to see how the plot changes considering only $N = 5$ modes. With $N = 5$ modes only, 5 resonances are considered in the model.



In this figure, the driving-point impedance found is plotted:

- in case 1, starting from the wave propagation solution;
- in case 2, using the modal superposition approach and considering $N = 8$ modes;
- in case 2, using the modal superposition approach and considering $N = 5$ modes.

For lightly damped systems at resonance, the resonant mode is dominating the system response. Therefore the approximation of the modal superposition approach is very good. On the contrary, at anti-resonance the approximation is worse than the actual solution obtained with the wave propagation approach. That's because in anti-resonance condition the system response is dominated by all modes. All the modes contribute to the system response: dealing with a finite number of modes, the approximation of the response is worse. Theoretically, if we had $N = \infty$ modes, the solutions would be exactly the same. It can be noticed that the approximation gets better if we increase the number of modes. The higher the number of considered modes:

- the larger the frequency range where the driving-point impedance is accurately approximated;
- the better the driving-point impedance is approximated in between two adjacent resonance minima.

The lower the number of considered modes, the more the anti-resonance frequency tends to be overestimated.

Fundamentals of Vibration Analysis and Vibroacoustics

Module 2 - Vibroacoustics of Musical Instruments

Assignment 2 - Experimental modal analysis of a violin

Bombaci Nicola 10677942

Fantin Jacopo 10591775

Intagliata Emanuele 10544878

June 2020

1) MATLAB code for modes identification

Starting from the experimental data collected into `Data.mat` file we implemented the MATLAB script for identifying the modes according to the procedure described in laboratory slides.

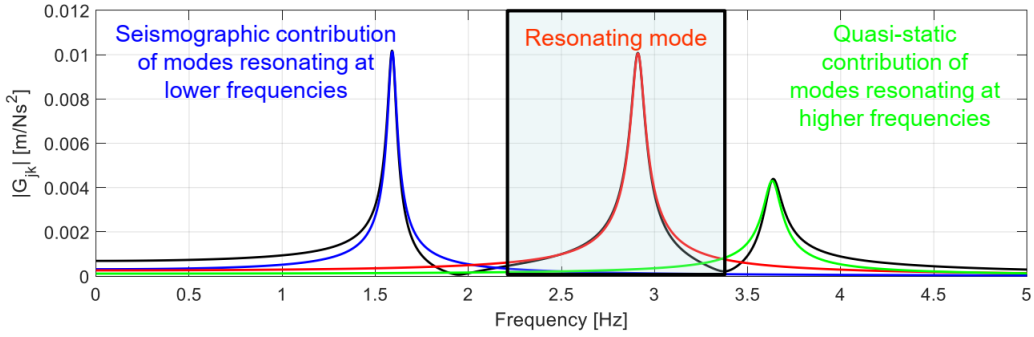
1a) Minimization algorithm

In order to study the vibrational modes of the violin starting from these experimental data, we refer to the **modal approach**, that describes the overall frequency response of a structure as superposition of N modes of vibration, as far as enough modes are considered:

$$G_{jk}^{\text{EXP}}(\omega) \approx \sum_{i=1}^N \frac{X_j^{(i)} X_k^{(i)} / m_i}{-\omega^2 + j2\omega_i \omega \xi_i + \omega_i^2} , \quad \xi_i = \frac{c_i}{2m_i \omega_i} \quad (1)$$

For well distinguished peaks and lightly damped structures, the FRF $G_{jk}(\omega)$ can be approximated around a certain ω_i as:

$$G_{jk}^{\text{NUM}}(\omega) \approx \sum_{i=1}^N \frac{A_{jk}^{(i)}}{-\omega^2 + j2\omega_i \omega \xi_i + \omega_i^2} + R_{jk}^H + \frac{R_{jk}^L}{\omega^2} , \quad \omega_{\text{inf}} < \omega_i < \omega_{\text{sup}} \quad (2)$$



The first thing we had to implement was an algorithm in order to find the frequency ranges of interest. We decided to divide the frequency axis in N partitions (where N is the number of identified peaks or considered modes).

Given the N peaks found (i.e. N maxima, see [2b]) we found $N + 1$ minima between those peaks (and the endpoints of the frequency axis).

Listing 1: Frequency range search

```

1 wp_dx = iini;
2 for yy = 1: (Nmodes + 1) % over the m(+1) peaks
3     wp_sx = wp_dx; % left end is former right end
4
5     if yy > Nmodes % right end
6         wp_dx = i_max;
7     else
8         wp_dx = indices(yy); % frequency of next peak (right
9             end)
10    end
11    [~, min_index] = min(abs(FRF_LP(wp_sx:wp_dx, :)), [], 1);
12    rfi(:,yy) = min_index + wp_sx - 1;
13 end

```

We obtain a set of $N + 1$ values of ω (i.e. the endpoints of the frequency ranges) for each measurement.

This is maybe not the most precise way to deal with this kind of problem but it can be seen in the last section that good results are delivered.

For a given set of experimental FRFs G^{EXP} , obtained for a fixed measurement location j and different excitation locations k (grid of points), a **least squares minimization procedure** can be implemented for the estimation of the **modal parameters** $(X^{(i)}, \omega_i, \xi_i, m_i)$.

Considering the experimental FRF matrix \mathbf{G}^{EXP} , it shows:

a number m of rows corresponding to the length of the frequency vector ω ;

a number n of columns corresponding to the $k - j$ pairs (i.e. the available FRFs).

Here we have that:

$G_r^{EXP}(\omega_s)$ is a generic element of the experimental FRF matrix \mathbf{G}^{EXP} corresponding to the r -th column (FRF) evaluated in correspondence of the frequency ω_s ;

$G_r^{NUM}(\omega_s)$ is the numerical FRF estimation around a certain ω_i , corresponding to the r -th column (FRF) evaluated in correspondence of the frequency ω_s , i.e.

$$G_k^{NUM}(\omega_s) = \sum_{i=1}^N \frac{A_r^{(i)}}{-\omega_s^2 + j2\omega_i\omega_s\xi_i + \omega_i^2} + R_r^H + \frac{R_r^L}{\omega_s^2}$$

1b) Error minimization problem

The **error function** to be minimized should then be:

$$\varepsilon = \sum_{r=1}^N \sum_{s=s_{\inf}}^{s_{\sup}} \Re^2\{G_r^{\text{EXP}}(\omega_s) - G_r^{\text{NUM}}(\omega_s)\} + \Im^2\{G_r^{\text{EXP}}(\omega_s) - G_r^{\text{NUM}}(\omega_s)\} \quad (3)$$

Since the error function depends non-linearly from the unknown parameters, an *iterative* minimization procedure must be used.

For an iterative procedure an **initial guess vector** x_0 is required, consisting of a preliminary estimate of:

ω_i which is found from the maximum peak in the considered frequency range (see section 2b);

ξ_i which is found through some simplified method, assuming that just the resonating mode is contributing to the system response. We used the **phase derivative method**:

$$\xi_i = -\frac{1}{\omega_i \frac{\partial \angle G_{jk}}{\partial \omega} \Big|_{\omega=\omega_i}}$$

$A_r^{(i)}$ which is found considering each FRF at resonance and assuming real valued mode shapes:

$$A_r^{(i)} \approx -\Im(2\xi_i \omega_i^2 G_r^{\text{EXP}}(\omega_i))$$

R_r^L and R_r^R are set to zero under the assumption of sufficiently distinguished peaks.

It can be seen that the non-linear minimization procedure elaborates *simultaneously* the whole set of FRFs, leading to an estimate of $\omega_i, \xi_i, A_r^{(i)}$. This is not a trivial problem from a computational point of view.

Firstly we tried to implement this procedure using `fminsearch` function. It finds the minimum of unconstrained multivariable function using derivative-free method. It is a nonlinear programming solver and searches for the minimum of a problem specified by

$$\min_x f(x)$$

where $f(x)$ is a function that returns a scalar, and x is a vector or a matrix.

In our case x is a set of modal parameters vectors (one for each measurement) and $f(x)$ should be the error function seen in eq. (3).

This approach led to a runtime of almost an hour.

In our second attempt we used the MATLAB function `lsqnonlin` (as suggested in laboratory slides). This function solves a non-linear least-squares curve fitting problem of the form:

$$\min_x \|f(x)\|_2^2 = \min_x (f_1(x)^2 + f_2(x)^2 + \dots + f_n(x)^2)$$

Rather than computing the value $\|f(x)\|_2^2$ (the sum of squares), `lsqnonlin` requires the user-defined function to compute the *vector-valued* function:

$$f(x) = \begin{bmatrix} f_1(x) \\ f_2(x) \\ \vdots \\ f_n(x) \end{bmatrix}$$

In other words, `x = lsqnonlin(fun, x0)` starts at the point `lsqnonlin(fun,x0)` and finds a minimum of the sum of squares of the functions described in `fun`. The function `fun` should return a vector (or array) of values and not the sum of squares of the values. The algorithm implicitly computes the sum of squares of the components of `fun(x)`.

This function forces us to use a slightly simplified version of the **error function**:

$$\varepsilon = \sum_{s=s_{\text{inf}}}^{s_{\text{sup}}} \Re^2\{G^{\text{EXP}}(\omega_s) - G^{\text{NUM}}(\omega_s)\} + \Im^2\{G^{\text{EXP}}(\omega_s) - G^{\text{NUM}}(\omega_s)\} \quad (4)$$

In this way the non-linear minimization procedure elaborates the FRFs *one-by-one*.

This leads us to a less precise minimization algorithm. On the other hand now it is much faster.

Using `lsqnonlin` we provide a `f(x)` of this form:

$$f(x) = \begin{bmatrix} f_1(x) \\ f_2(x) \end{bmatrix} = \begin{bmatrix} \Re\{G^{\text{exp}}(\omega_s) - G^{\text{num}}(\omega_s)\} \\ \Im\{G^{\text{exp}}(\omega_s) - G^{\text{num}}(\omega_s)\} \end{bmatrix}$$

Remember: the algorithm implicitly computes the sum of squares of the components of `f(x)`.

Listing 2: Snippet of code from `err_i.m`

```

1 % error computation
2 c_e = H_exp - H_num; %complex error
3 real_e = (real(c_e));
4 imag_e = (imag(c_e));
5 error = [real_e; imag_e];

```

In the end the minimization process gives us an estimation of the modal parameters $\xi_i, \omega_i, X^{(i)}, R_r^L$ and R_r^R .

Setting $m_i = X_r^{(i)}$, the normalized mode shape at each of the k locations is given by the gain $A_r^{(i)} = X_r^{(i)}$. Other useful modal parameters can be found in function of the previous ones:

$$c_i = 2m_i\omega_i\xi_i$$

$$k_i = \omega_i^2 m_i$$

1c) FRF Reconstruction

The FRFs are reconstructed using the custom function `reco.m`. It takes as input a vector with modal parameters and gives as output the reconstructed FRF, using the formulation seen in eq. (1).

Listing 3: Snippet of code from `reco.m`

```

1 for mm = 1:meas
2     for pp = 1:nPeaks
3         FRF_reco(:, mm) = FRF_reco(:, mm) + ...
4             (A_j(pp,mm) + 1i*B_j(pp,mm))./(- m_i(pp
5                 ,mm).*omega.^2 + 1i*c_i(pp,mm).*omega +
6                     k_i(pp,mm));
7     end

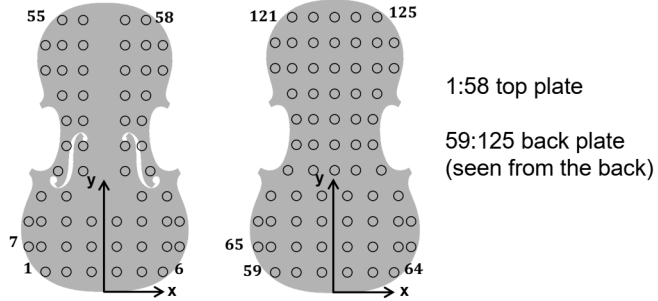
```

Quality of the estimates can be visually assessed comparing in a plot the identified FRFs G^{NUM} with the experimental ones G^{EXP} . We will see it in the next sections.

2) Software testing

2a) Data pre-processing

The given `Data.mat` file contains experimental FRFs [m/s^2N] that have been obtained performing a hammer test on a violin, following a roving hammer procedure, that consists in fixing the measurement position(s) while varying excitation location. The coordinates of the measuring grid can be found in the variable `xy`. The measuring grid is reported in the figure below.



To sum up, `Data.mat` contains the frequency vector (`freq`), the experimental FRF matrix (`FRF`, measurement direction positive outward with respect to the top plate), the measurement grid (`xy`), the contours of front plate (`xy_bt`) and back plate (`xy_bf`).

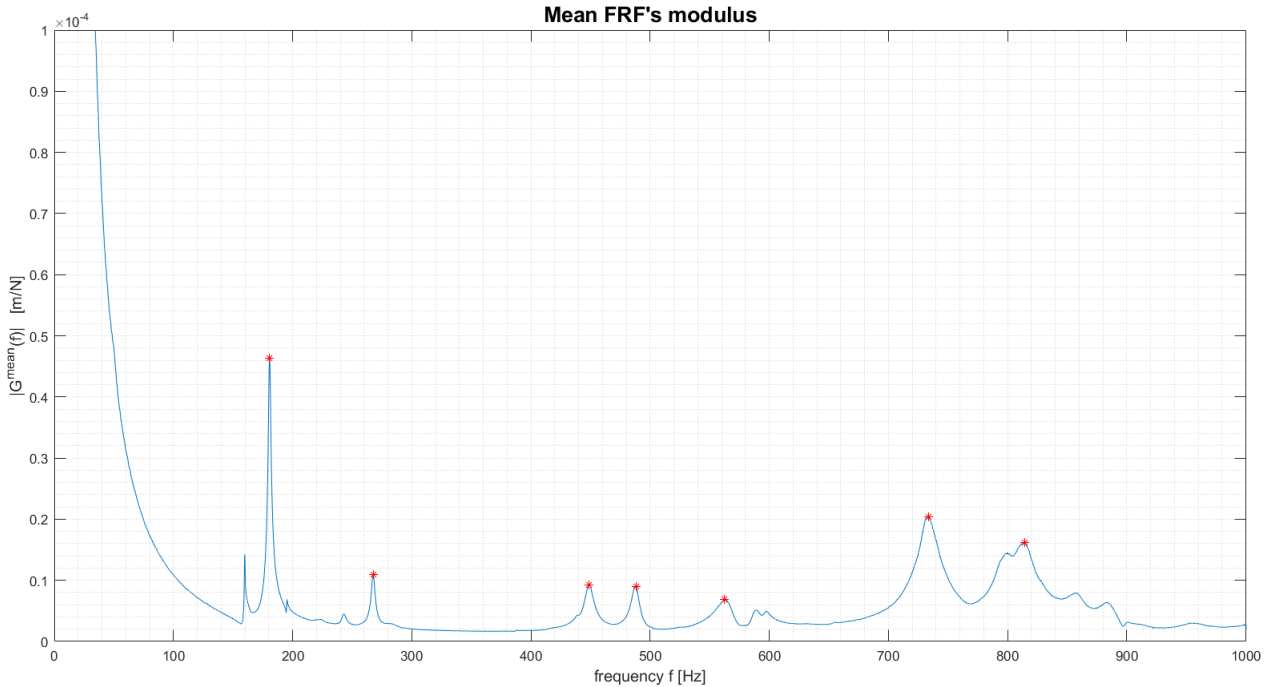
First of all we converted the unit of measurement of the FRFs from an acceleration over a force [m/s^2N] to a displacement over a force [m/N]. To do so we divided the FRFs by the vector ω^2 using the function `repmat`.

Being the frequency response spectra very noisy, we decided to smooth them out, extracting only the envelope.

2b) Peak search

The steps we followed to identify the resonance frequencies, which correspond to the relative maxima of the module diagram of the FRFs:

- Computing the mean FRF over all the low-passed FRFs, considering those measured for points on the front plate together with those for points on the back plate, and we low-passed again the result. This way, we would be quite sure to identify vibration modes in common between the two plates.



- Using `findpeaks` to identify the most evident maxima in the mean FRF. In particular, the following snippet of code is used for searching for peaks.

Listing 4: Peaks' search

```

1      prom = 0.000003;
2      width = 8;
3      tr = 0;
4      iini = 500;
5      [~, indices] = findpeaks(FRFmean(iini:
6          end), 'MinPeakProminence', prom,
7          'MinPeakWidth', width, '
8              Threshold', tr);
Nmodes = length(indices);
indices = indices + iini;

```

As it can be seen the first 500 samples are discarded in order not to consider the initial part of the FRF that diverges. This can be attributed to the structure used for holding the violin, so we're allowed to pretend the FRF starts after this region.

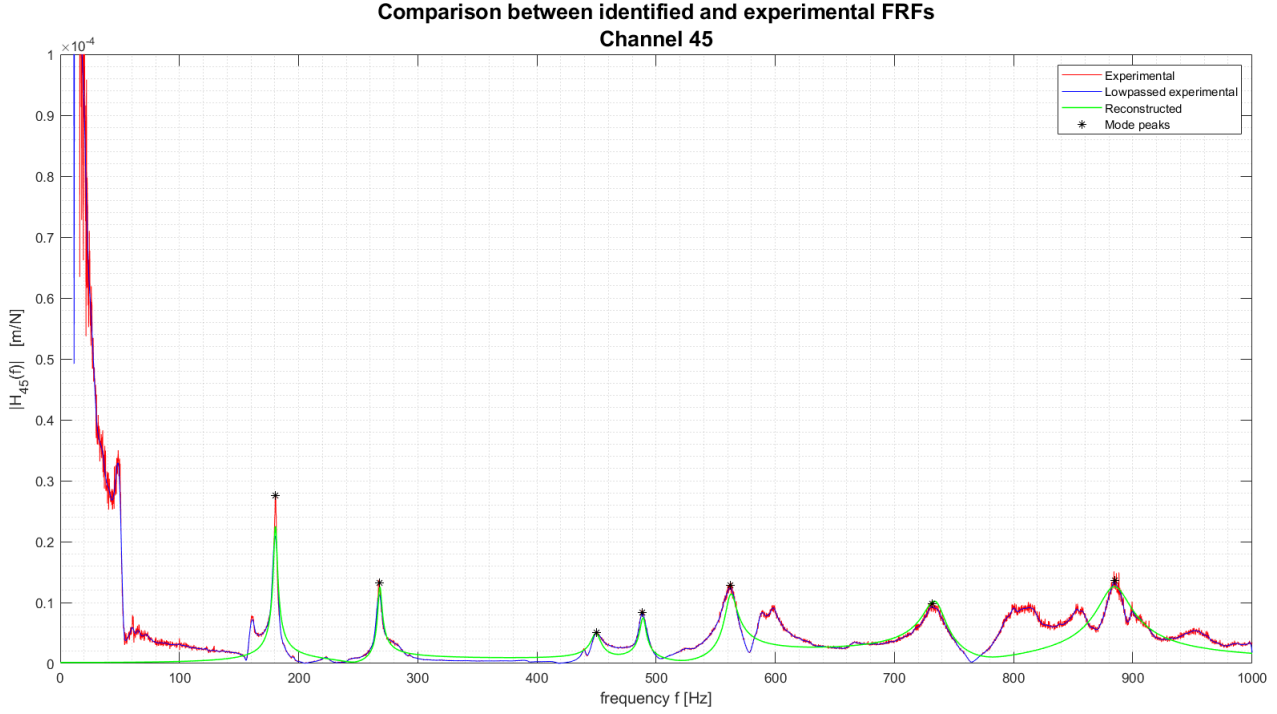
- Finding the frequency value associated with each peak. These constitute the first-guess-values for the minimization process as for the natural frequencies.

3) Results

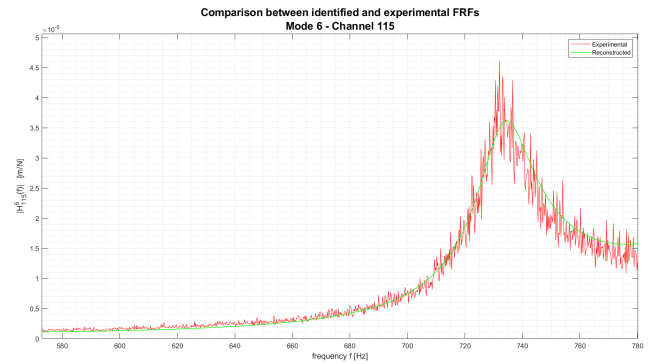
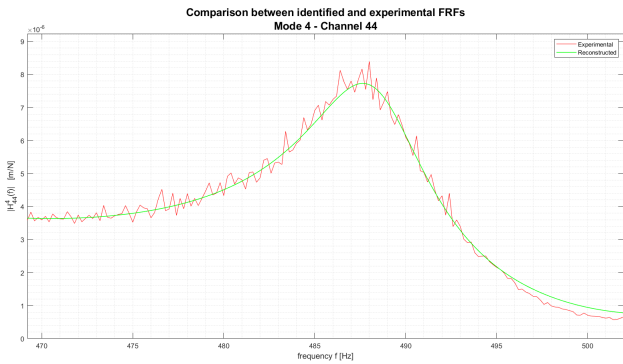
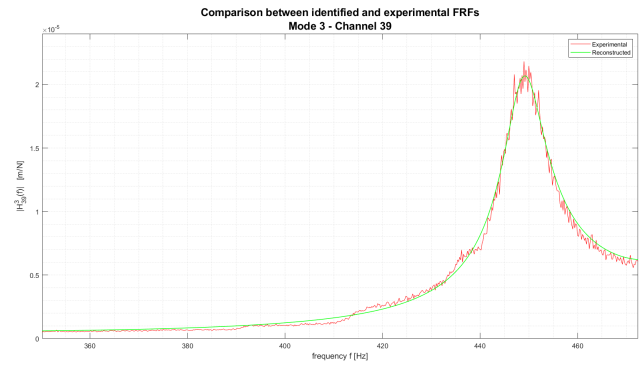
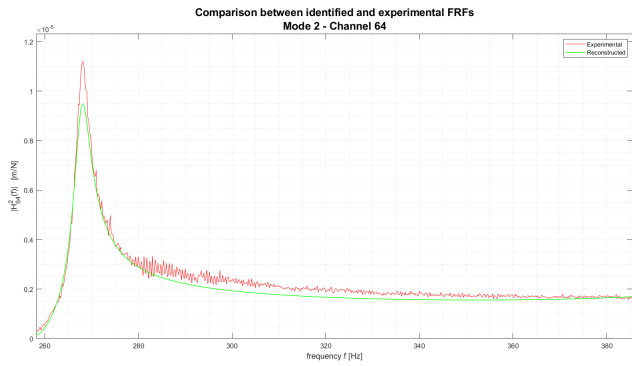
3a) Comparison between reconstructed and experimental FRFs

Our MATLAB script identifies 7 modes. Considering one of the 125 input-output couples, we report the reconstructed Frequency Response Function compared to the corresponding experimental one. The numerical one provides a good approximation of the original one, following its amplitude envelope. We also remind that, in case the value of the modulus for one of the identified natural frequencies is not the maximum value in the considered

frequency range, we considered the actual maximum value, and its corresponding frequency, for the reconstruction of that portion of FRF. This is the case for the last peak in the showed diagram, whose frequency is 884 Hz in place of 814 Hz.



Taking a closer look at some of the identified vibration modes for some of the measurements, we may appreciate even more the fact a non-noisy FRF has been analitically obtained:



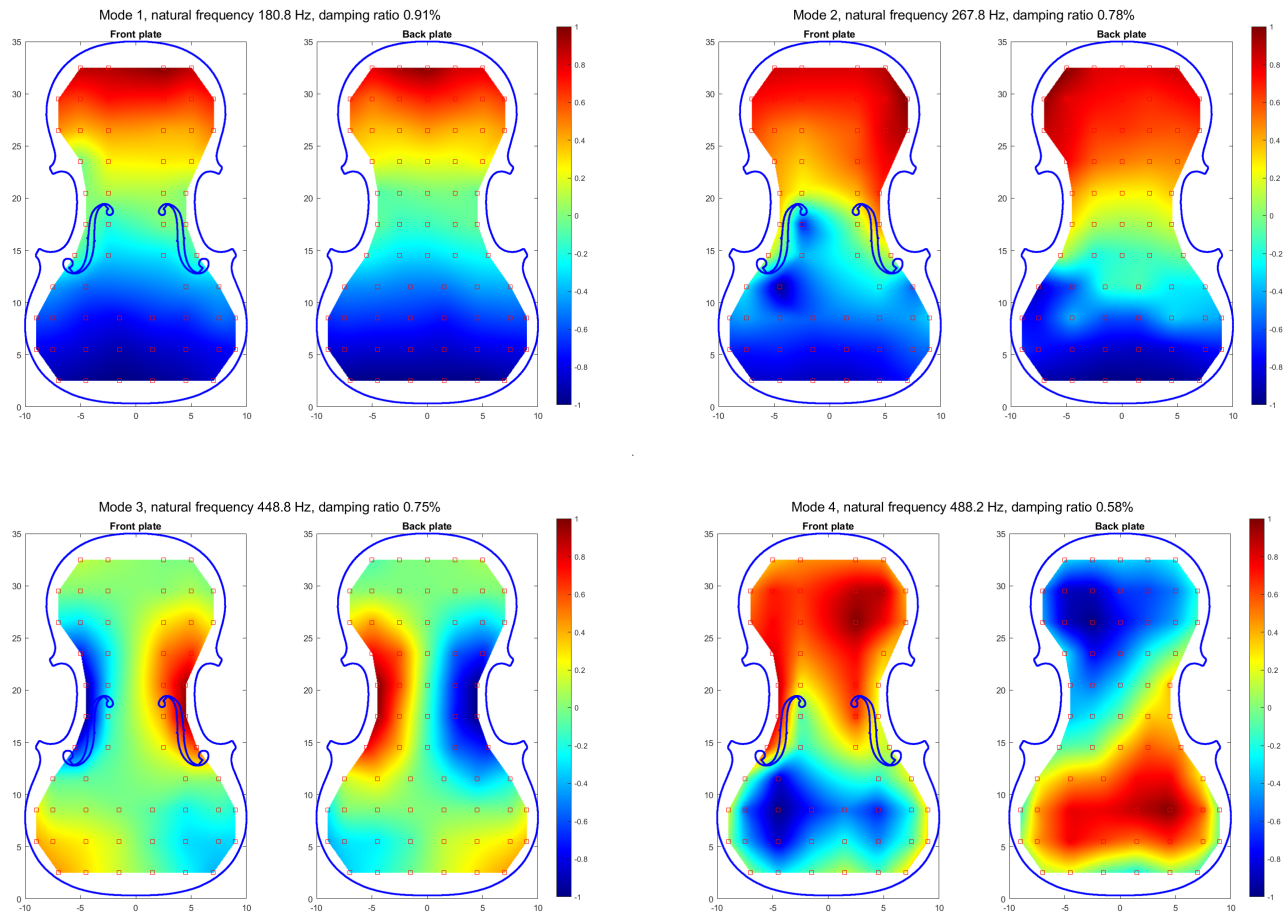
3b) Modal parameters

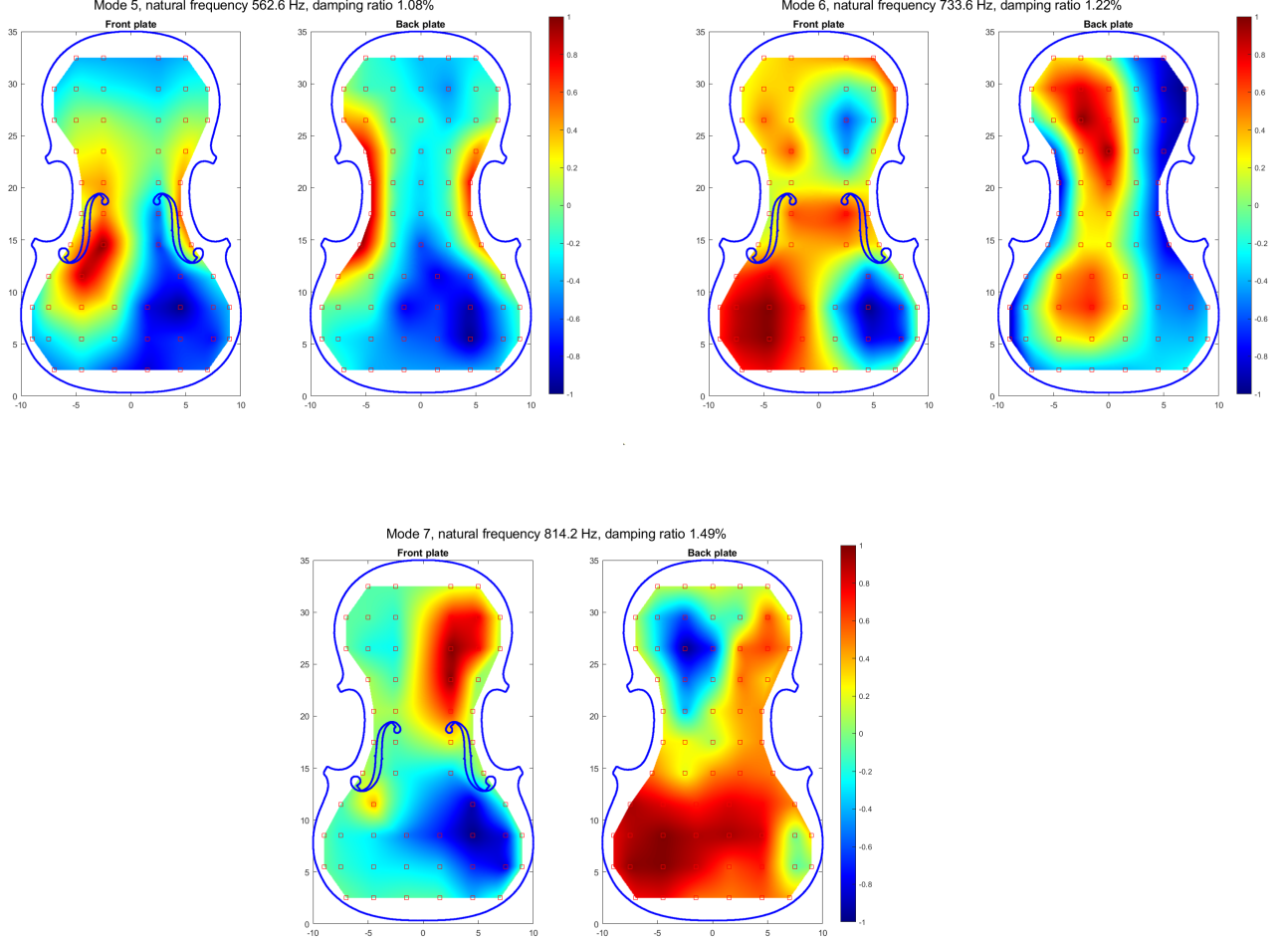
The results in terms of natural frequencies and damping ratios for the 7 identified modes can be summarized in the following table.

Mode	Frequency [Hz]	Damping ratio (%)
1	180.8	0.91%
2	267.8	0.78%
3	448.8	0.75%
4	488.2	0.58%
5	562.6	1.08%
6	733.6	1.22%
7	814.2	1.49%

3c) Identified modes

The following plots summarize the characteristics of the vibration modes of the violin plates: for each of them, we're displaying natural frequency, adimensional damping ratio (percentage) and a graphical representation of the mode shape, indicating the displacement of the points on the surface with respect to each other for that particular oscillation mode.





As we could infer a priori, the mode shape is more and more complex as the resonating frequency increases: in the first two modes, we can easily identify two main oscillating areas (the upper part and the lower part of the plate), in accordance between top and back plate. In the third one, there are four, with crossed polarization and accordance between top and back plate, and so on. As the mode number increases, the two plates start decouple one from the other, and the oscillation modes may not correspond anymore. This is due to the fact the higher the frequencies, the more top and back plate exhibit different modes. Talking about the damping ratio, this is on average lower at lower frequencies than at higher ones.